Numerical optimization of three-dimensional coils for NSTX-U

IOP Publishing Plasma Physics and Controlled Fusion

Plasma Phys. Control. Fusion **57** (2015) 104001 (8pp) doi:10.1088/0741-3335/57/10/104001

Numerical optimization of three-dimensional coils for NSTX-U[3]

S A Lazerson[1], J-K Park[1], N Logan[1] and A Boozer[2]

[1] Princeton Plasma Physics Laboratory, Princeton, NJ 08540, USA
[2] Columbia University, New York, NY 10027, USA

E-mail: lazerson@pppl.gov

Received 30 January 2015, revised 2 April 2015
Accepted for publication 9 April 2015
Published 3 September 2015

Abstract

A tool for the calculation of optimal three-dimensional (3D) perturbative magnetic fields in tokamaks has been developed. The IPECOPT code builds upon the stellarator optimization code STELLOPT to allow for optimization of linear ideal magnetohydrodynamic perturbed equilibrium (IPEC). This tool has been applied to NSTX-U equilibria, addressing which fields are the most effective at driving NTV torques. The NTV torque calculation is performed by the PENT code. Optimization of the normal field spectrum shows that fields with $n = 1$ character can drive a large core torque. It is also shown that fields with $n = 3$ features are capable of driving edge torque and some core torque. Coil current optimization (using the planned in-vessel and existing RWM coils) on NSTX-U suggest the planned coils set is adequate for core and edge torque control. Comparison between error field correction experiments on DIII-D and the optimizer show good agreement.

Keywords: tokamak, equilibrium, optimization, torque, rotation, in-vessel coils

(Some figures may appear in colour only in the online journal)

1. Introduction

The utility of three-dimensional (3D) perturbative coils on tokamaks for torque control has motivated exploration of a new set of in-vessel coils on the NSTX-U device [1]. The compensation of error-fields, control of magnetohydrodynamic (MHD) modes and control of resistive modes has driven the installation of non-axisymmetric coils on many modern tokamaks. A recent desire for control of externally applied torques with 3D fields has initiated a reassessment of the proposed Non-axisymmetric Control Coils (NCC) coils for NSTX-U (figure 1). Such a capability would allow access to low-rotation regimes predicted for ITER and future energy producing reactors. The design of perturbative coils has previously been determined by a desire to control toroidal mode number, coupled with engineering constraints. This has resulted in relatively simple coils for many existing machines. For this work a model based approach was taken where the fields were optimized to a desired plasma response, producing a desired poloidal and toroidal spectrum. This optimized spectrum may then be used to determine the design of the coils themselves.This approach is analogous to stellarator design and borrows many of the stellarator tools. The IPECOPT code has been developed reusing many of the subroutines found in STELLOPT [2]. The non-linear ideal MHD model found in STELLOPT (VMEC) [3], has been replaced with the Ideal Perturbed Equilibrium Code (IPEC). The IPEC code solves a linear perturbed ideal MHD equilibrium model [4]. In this work, the Neoclassical Toroidal Viscosity (NTV) torque as calculated by the Perturbed Equilibrium Non-ambipolar Transport (PENT) code [5] was chosen as the target quantity to optimize. The resulting tool has been applied to NSTX-U equilibria exploring the possibility of a new set of perturbative coils and evaluating the existing set.

[3] Notice: This manuscript has been authored by Princeton University under Contract Number DE-AC02-09CH11466 with the U.S. Department of Energy. The publisher, by accepting the article for publication acknowledges, that the United States Government retains a non-exclusive,paid-up, irrevocable, world-wide license to publish or reproduce the published form of this manuscript, or allow others to do so, for United States Government purposes.

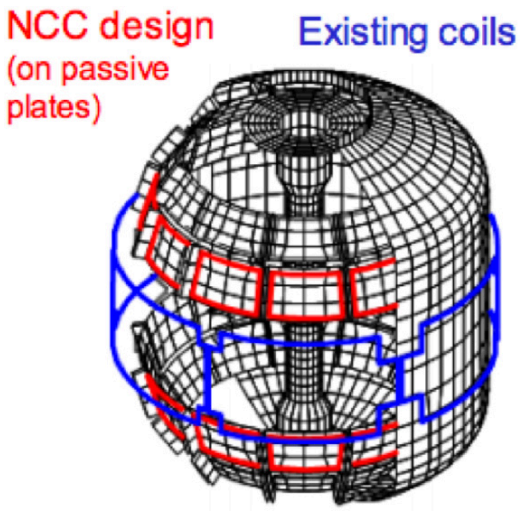

Figure 1. Depiction of the NSTX-U vessel, passive plates and perturbative coil. The Resistive Wall Mode (RWM) coils (blue) already exist on the machine, while the Non-axisymmetric Control Coils (NCC, red) are planned for the future.

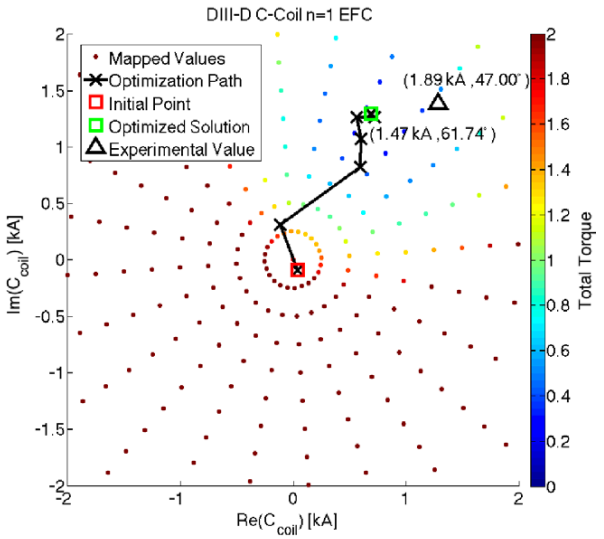

Figure 2. Polar plot showing mapping and optimization of DIII-D error field correction experiment. Dots indicate amplitude of PENT calculated total torque, with position indicating phase and amplitude of applied $n = 1$ C-coil field. Optimization path shows how IPECOPT moves through this space. Discussion of experimental optimization of C-coil currents is found in [29].

Three dimensional fields already play a large role in tokamak operations. The value of non-axisymmetric coils was first demonstrated through their ability to compensate error fields and thus avoid locked modes [6–8]. Experiments on DIII-D indicated that applied 3D fields were beneficial to confinement. The extension of 3D fields to mode control has also been well documented. The NSTX and DIII-D devices have demonstrated the ability to operate above the no-wall beta limit through resistive wall mode control [9–11]. Additionally, the use of 3D fields for edge localized mode (ELM) control has been extensively documented [12–14]. Control of such modes is crucial to ITER (and future reactors) as the associated heat loads could damage the device [15, 16]. As ITER will be a low rotation device, recent efforts have focused on slowing toroidal rotation in current devices using 3D fields [17]. This can be achieved through the mechanism of NTV torque. This work seeks to evaluate which 3D fields drive the most amount of NTV torque in the NSTX-U device.

Given the large number of modern tokamaks which employ perturbative coils, designs and implementations remain rather simple. Early coils were simple loops placed on the outside of the device in an attempt to validate locked-mode models. The first perturbative coil placed on DIII-D was a simple dipole coil, later replaced with a 6-fold picture frame coil set. Many machines have external coils which were easy to implement and allowed for correction of large error fields. These coil sets also led to the demonstration of ELM suppression by 3D fields and operation above the no-wall beta limit. Spurred by interest in ELM control many devices have upgraded to in-vessel coils. These coils allow for variation of the applied field pitch through relative phasing of the two rows. The design of these coil sets were limited by engineering constraints and lack of modeling showing benefits of more complex coil sets. The exception to these examples being the TEXTOR device and its dynamic ergodic divertor [18]. In this work we bridge that gap by calculating an optimized set of normal fields which provide a desired plasma response.

A parallel can be drawn between perturbative coil design and stellarator design, suggesting a code built upon the existing stellarator tools. Stellarator design begins with the choice of plasma shape which results in the optimum stellarator, as calculated by various metrics. Once the shape has been determined, codes such as NESCOIL [19] and COILOPT [20] can be used to determine a coil set which provides an adequate normal field to produce said magnetic geometry. In IPECOPT, the linear perturbed ideal MHD equilibrium is determined by a set of vacuum B-normal fields on the axisymmetric boundary. The vacuum harmonics serve as our free parameters in the optimization. These fields provide the desired plasma response, in our case NTV torque. The optimum vacuum fields may then be fed into the coil optimization codes to determine the optimized coilset. The IPECOPT code may also be used to directly evaluate the optimal coil currents given a fixed coil geometry. In section 2 the IPECOPT code is described in detail. Section 3 presents the results of optimizing the NSTX-U perturbed equilibria, with a followup discussion in section 4.

2. Method

The desire to examine the possibility of more sophisticated coil sets on NSTX-U motivated the development of an optimizer based around the linear perturbed ideal MHD equilibrium code IPEC. The IPEC code has a demonstrated utility and predictive capability for perturbed tokamak equilibria. This capability includes the suppression of ELMs and calculations of NTV torque. In the case of NTV torque, the PENT code (equilibria calculated by IPEC) has proven useful in

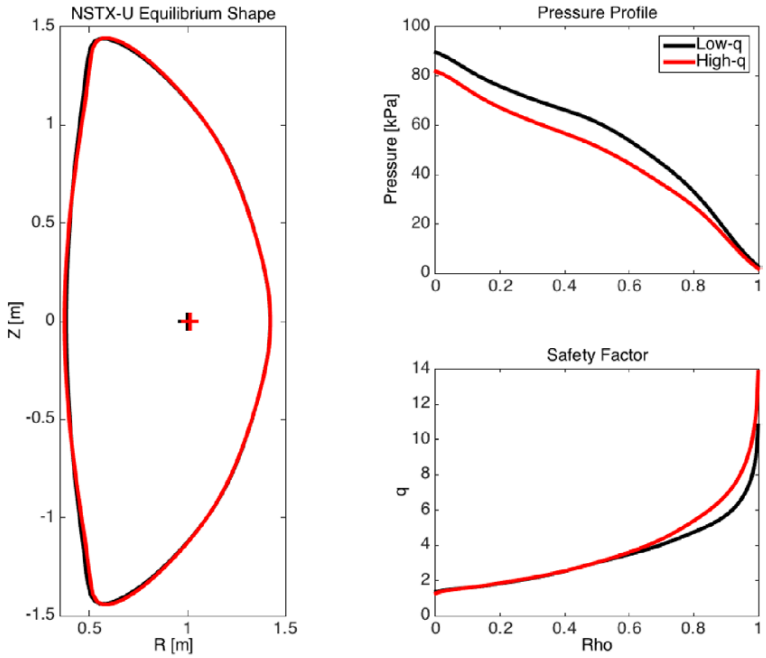

Figure 3. NSTX-U H-mode equilibrium utilized for torque optimization. The Low-q equilibrium has $\beta = 12.6\%$ and $I_p = 2.0$ [MA]. The High-q equilibrium has $\beta = 10.4\%$ and $I_p = 1.6$ [MA]. Such equilibria are representative of the enhanced capabilities in NSTX-U.

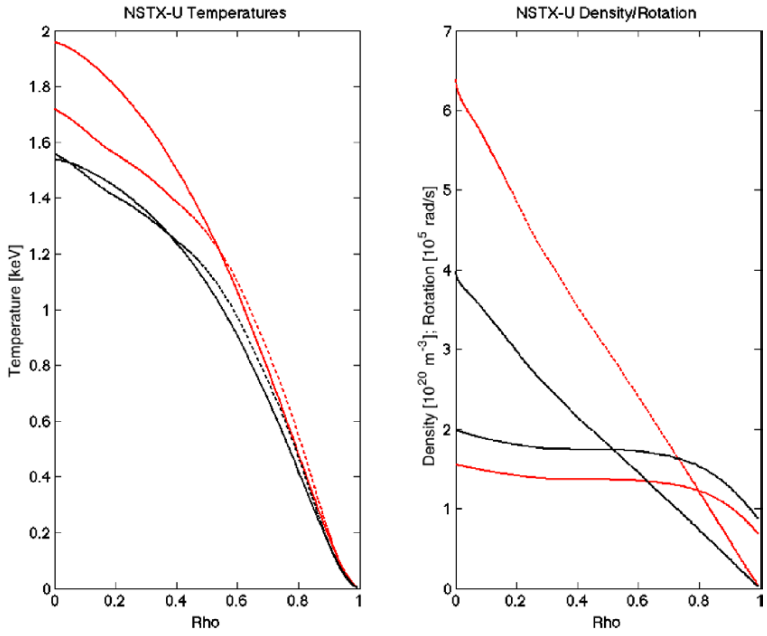

Figure 4. NSTX-U temperature and density profiles for high q-edge ($I_p = 1.6$ [MA], red) and low q-edge ($I_p = 2.0$ [MA], black) cases. Electron temperature and rotation are indicated with dashed lines. Ion temperature and density are indicated with solid lines.

predicting error field correction for the DIII-D tokamak. Such results motivated the notion of using a optimization technique for perturbative coil design, similar to what is done for stellarators. From such considerations the IPECOPT code was developed as a recoding of the STELLOPT code.

The IPEC code calculates perturbed ideal MHD equilibrium using an inverse representation. The code solves the following equation

$$\nabla \delta p = \delta \vec{j} \times \vec{B}_0 + \vec{j}_0 \times \delta \vec{B} \tag{1}$$

where p is the plasma pressure, $\vec{j}$ the current density, $\vec{B}$ the magnetic field, δ denotes a perturbed quantity and the subscript 0 denotes the underlying axisymmetric equilibrium quantity. The equations are solved by utilizing matrices calculated by the DCON stability code [21]. It is important to note that

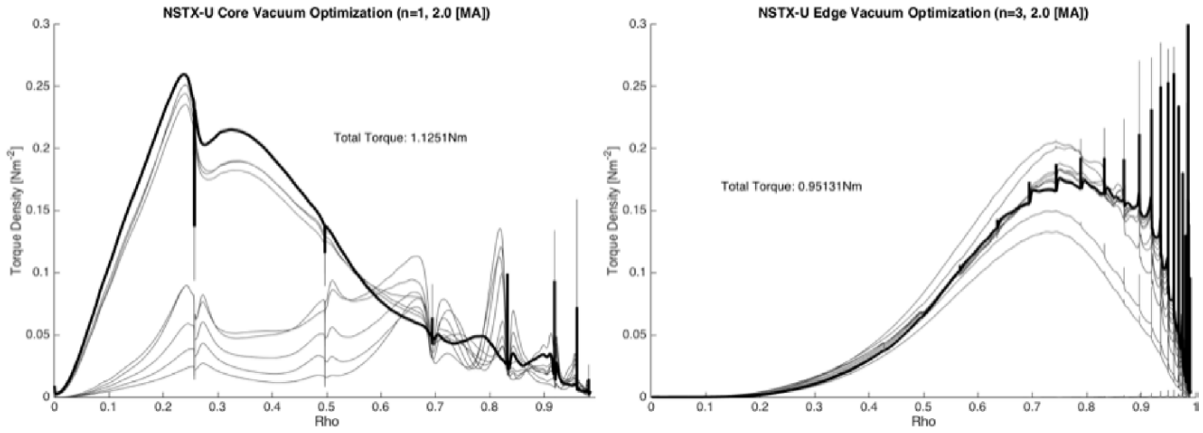

Figure 5. Optimization of NSTX-U normal field harmonics for torque density profile (core left, edge right). The thin black lines depict the various interim profiles found during the optimization while the thick black line depicts final optimized profile. Total torque values are around 1 Nm.

this equation neglects the effects of rotation, which is clearly important for stability [22]. Inclusion of flow into the linear perturbed model of IPEC is an ongoing area of code development. The perturbing fields are specified in terms of poloidal Fourier harmonics for a given toroidal mode number (in user selectable straight field line coordinates). This allows the total or vacuum field to be specified on the plasma boundary. It should be noted that care must be taken to avoid normal field distributions which are large and may break the linearity assumptions of the code. Both arbitrary vacuum fields or those supplied by a set of discrete coils can be specified on input. For this work a poloidal spectrum ranging from $m = [-12, 27]$ was considered with the underlying equilibrium truncated at flux 0.98. A PEST coordinate system was utilized as this has shown the best spectral qualities for the NSTX-U configurations considered [23]. The resulting equilibrium possesses a finite magnetic field normal to the underlying axisymmetric flux surface. This field may then be used with other codes to evaluate various physics parameters.

One such physics parameter is the torque related to non-ambipolar transport as calculated by the PENT code. This code utilizes the magnetic fields from the IPEC calculation and the underlying equilibrium profile information (temperature, density and rotation) to calculate the resulting torque. This is achieved by solving the following drift-kinetic equation using the IPEC magnetic fields [24, 25]

$$T_\phi = -\frac{n^2}{\sqrt{\pi}}\frac{R_0}{B_0}\int \mathrm{d}\psi NT \int \mathrm{d}\Lambda \bar{\omega}_b |\delta\bar{J}_l|^2 \int \mathrm{d}x \Re_{Tl} \qquad (2)$$

Here n is the toroidal mode number, R_0 is the major radius, B_0 the toroidal field, N the particle number density, T the temperature and $\bar{\omega}_b = \omega_b R_0/\sqrt{2xT/M}$ the normalized bounce frequency. The left most integral is over the toroidal flux and accounts for the finite beta effects. The middle integral is the perturbed action ($\delta\bar{J}_l$) integrated over the normalized particle magnetic moment ($\Lambda = \mu\ B_0/E$). The power of two over the perturbed action brings in a nonlinearity to the calculation, despite the linearity in the underlying equilibrium. The perturbed action is calculated as:

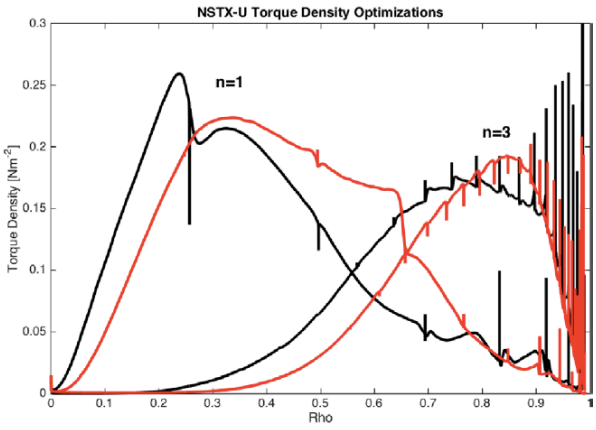

Figure 6. Torque density profiles resulting from optimization of normal field boundary harmonics. The 1.6 MA (red) and 2.0 MA (black) cases are plotted for core ($n = 1$) and edge ($n = 3$) optimizations. As current is increased in NSTX-U profiles becomes more peaked in the core and less peaked in the edge.

$$\delta J_l = \int \mathrm{d}V \frac{JB}{v_\parallel} P_l^{\pm 1}\left[(2E - 3\mu B)\frac{\delta B}{B} + (2E - 2\mu B)\frac{1}{J}\nabla\cdot\xi\right] \qquad (3)$$

where $J = (\nabla\psi \times \nabla\theta \cdot \nabla\alpha)^{-1}$ is the Jacobian, B is the magnetic field strength, $v_\parallel$ the parallel particle velocity, E the energy, μ the magnetic moment, $P_l^{\pm 1}$ the Legendre polynomials and ξ the displacement. The normalization of this quantity gives $\delta\bar{J}_l^2 = \delta J_l^2/2xT\ M\ R_0^2$. The right most integral in the torque equation is an integral over the normalized energy ($x = E/T$), computed as:

$$\Re_{\mathrm{TL}} = \frac{\left[\omega_\phi + \omega_{*T}\left(x - \frac{5}{2}\right)\right]x^{5/2}\mathrm{e}^{-x}}{\mathrm{i}[(l - \sigma nq)\omega_b + n(\omega_E + \omega_D)] - \nu_i} \qquad (4)$$

where ν is the collision frequency, ω_ϕ the rotation frequency, ω_b the bounce frequency, ω_E the $E \times B$ frequency, ω_D the diamagnetic drift frequency and x the normalized energy. Here

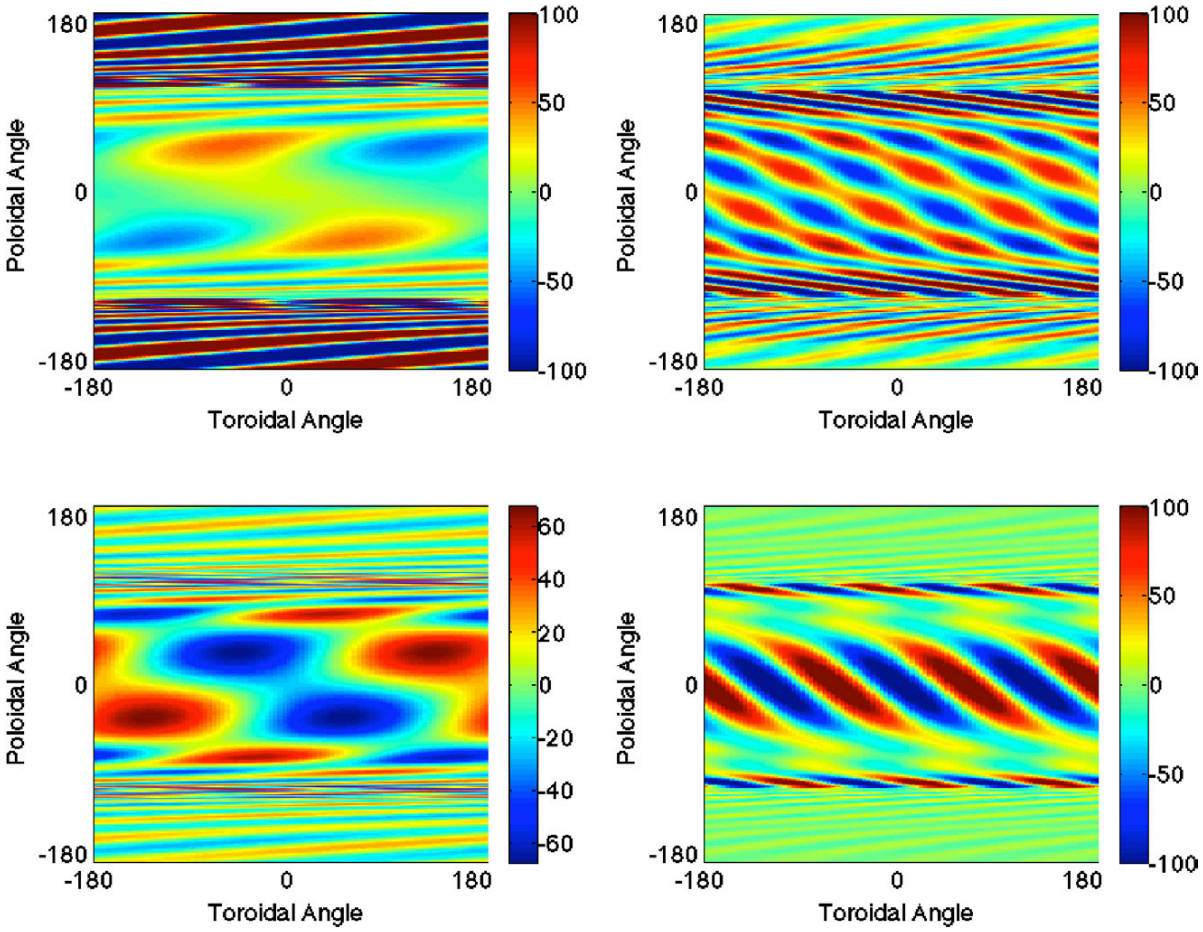

Figure 7. Optimized normal magnetic field for the $n = 1$ low q (upper left), $n = 1$ high q (lower left), $n = 3$ low q (upper right) and $n = 3$ high q (lower right) equilibria. Here the poloidal angle is measured from the outboard mid-plane (0°). The total field (vacuum + plasma response) is plotted. The normal field is plotted in Gauss [G].

resonances arise from the term $[(l - \sigma\, nq)\omega_b + n(\omega_E + \omega_D)]$, these are particles which see the same fields over and over again. In this formulation torque is a consequence of neoclassical nonambipolar transport where momentum is exchanged through the electromagnetic fields. The nonlinearity of the torque as calculated by PENT suggested that to find the optimum set of fields to drive torque a non-linear optimization technique would be required.

The IPECOPT code was developed to optimize the choice of normal fields in IPEC to a set of target parameters. The goal of such a code is analogous to that of another well established stellarator optimization code STELLOPT. To this end many of the optimization routines (Levenberg–Marquardt [26], Differential Evolution [27], Particle Swarm [28], Mapping) were reused, significantly reducing much of the work necessary to develop an optimizer. The result is a functionally parallelized optimizer based around IPEC. Two types of quantities may be optimized in the code: the normal field boundary harmonics, or the perturbative field coil currents. In the former, the optimizer directly varies the boundary harmonics, which can represent the total (plasma and external) or external field (user's choice). In the latter case, the current amplitude and phasing of a given row a coils is optimized. This specification is necessary as the linear nature of IPEC treats each toroidal mode number independently. The NTV torque density profile was chosen as the target to fit.

As a demonstration of the code's capabilities an error field scan experiment in DIII-D was replicated by the code. In this demonstration, error fields were included in the IPEC modeling through the SURFMN code [30] and phase and amplitude of the C-coil's $n = 1$ field was allowed to vary. The SURFMN code provides an approximate model of the error field in DIII-D. This is input into the plasma response model to get the true error field. The IPECOPT code was then run in mapping mode with total torque as calculated by the PENT code being output. The mapping mode in IPECOPT allows a gridded N-dimensional search of parameter space to be performed. Figure 2 depicts the phase and amplitude scan which was mapped (two dimensional space). The optimizer was then run in Levenberg mode starting from a poor initial condition (100 [A],~310° phase) and targeting a zero torque density profile. The resulting path the optimizer took through the two-dimensional space of coil current amplitude and phase is over plotted. The results suggest fair agreement between the optimized choice of coil currents and the experimental value, given the approximation made using a SURFMN vacuum

Table 1. Coil current optimization showing phase and amplitude of applied fields.

	$n = 1$ Core	$n = 1$ Edge	$n = 3$ Core	$n = 3$ Edge
Upper NCC	1260 A-t @ −17°	7850 A-t @ −123°	577 A-t @ −10°	2060 A-t @ −95°
RWM	2040 A-t @ 36°	656 A-t @ 167°	1800 A-t @ 54°	1080 A-t @ 109°
Lower NCC	1810 A-t @ 94°	5640 A-t @ 45°	573 A-t @ 10°	2520 A-t @ 79°

Note: Note that the $n = 1$ edge optimization failed to achieve a interesting torque profile. In addition, the $n = 1$ edge optimization has coil current amplitudes greater than possible in experiment. Phase with respect to RWM coil phasing.

error field and fixed rotation and species profiles. It should also be noted that the optimization agreed with the mapping. This demonstrates that the optimizer is working correctly.

As the IPEC code requires an underlying equilibrium, optimization of the NSTX-U perturbative coil set began by choosing two modeled NSTX-U equilibria to work with. Figure 3 depicts the two equilibria used in this analysis. These equilibria are representative of high ($I_p = 1.6$ [MA]) and low edge-q ($I_p = 2.0$ [MA]) configurations and of the larger current drive scenarios expected in the experiment. In this work both the Fourier harmonics of the normal field spectrum and proposed coil set were examined. Attention was paid to $n = 1$ and $n = 3$ toroidal field spectrums examining both the possibility of driving core and edge torque densities. The PENT code required species density and rotation profiles (figure 4). It should be noted that the profiles were held fixed so the possibility of transport response in experiment remains.

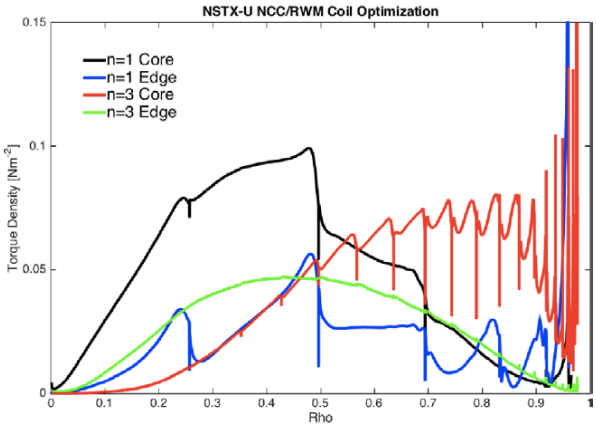

Figure 8. Torque profiles obtained from optimization of NCC and RWM coil currents. The $n = 3$ waveform indicates an ability to drive both an edge torque and a broad torque peaked at $\rho = 0.5$. Target total torque for these runs was ∼0.5 Nm.

3. Results

In this work optimization of the applied normal fields to the NSTX-U equilibrium indicated that an ability to drive core torque with applied $n = 1$ fields and edge torque with $n = 3$. This result held for both the optimization of the applied normal field spectrum and optimization of the NCC and RWM coil currents. The $n = 1$ fields did not appear capable to driving edge torque. Targeting core torque in the optimization the $n = 3$ fields did drive a broad torque (somewhere between edge and core torque profiles), but at reduced efficiency (lower total torque for a given applied field strength). These results suggest that, with the full NCC coils and the RWM coils, torque profile control in NSTX-U should be possible. These optimizations significantly extend the utility of the proposed NCC coil set.

Optimizations were performed targeting a step function like torque density profile. The choice of this profile was motivated by a lack of a-priori knowledge of what the torque density profile should look like. This motivated targeting a simple profile which biased the optimization either towards edge or core torque density. The amplitude of the target was chosen to be consistent with estimates of NBI torque in NSTX-U [31]. This worked well with the $n = 1$ simulation initially showing a edge biased profile which becomes increasingly core biased as the optimization progresses (figure 5). The highly localized spikes present in the torque density are attributed to resonant response at the low order rational surfaces. Experimental evidence suggests that one should be skeptical of fine scale detail in this profile. In a loose sense the spikes are a measure (or rather artifact) of resonant field drive. From their reduction in amplitude it can be inferred that the optimization was both fitting the torque density profile and minimizing the amount of unnecessary resonant field drive. The $n = 1$ case shows that some level of resonant field drive is necessary to drive torque deeper in the plasma, while near the edge resonant behavior is decreased. So without explicitly minimizing the resonant field drive, resonant fields were minimized. It should be noted that explicit minimization of low order resonances is possible but left to future work.

Optimization of the applied normal field Fourier harmonics indicated that torque density profiles could be created which were distinctly localized to the core or edge of the plasma. These optimizations were performed using the modified Levenberg–Marquardt method in IPECOPT. This method requires that the number of targeted parameters exceeds the number or free parameters (in these optimization the 40 harmonics). Figure 6 depicts the resulting torque density profiles for each equilibrium examined. The $n = 3$ profiles are peaked around the $\rho = 0.8$ region of the plasma. The simulations suggest that as q increases in the edge region, the ability to drive edge torques does not change significantly. It would appear that as q increases the edge torque profile becomes slightly more peaked. Core torque optimizations suggest a greater sensitivity to equilibrium changes. The low q case had a torque density profile peaked inside of $\rho = 0.5$, while the high q case had a much broader torque profile. Both $n = 1$ cases indicate significantly reduced edge torque when compared to the $n = 3$ cases.

The magnetic field which produced these profiles shows distinct features (figure 7). Each equilibrium suggests field strengths which are attainable with modern in-vessel coil

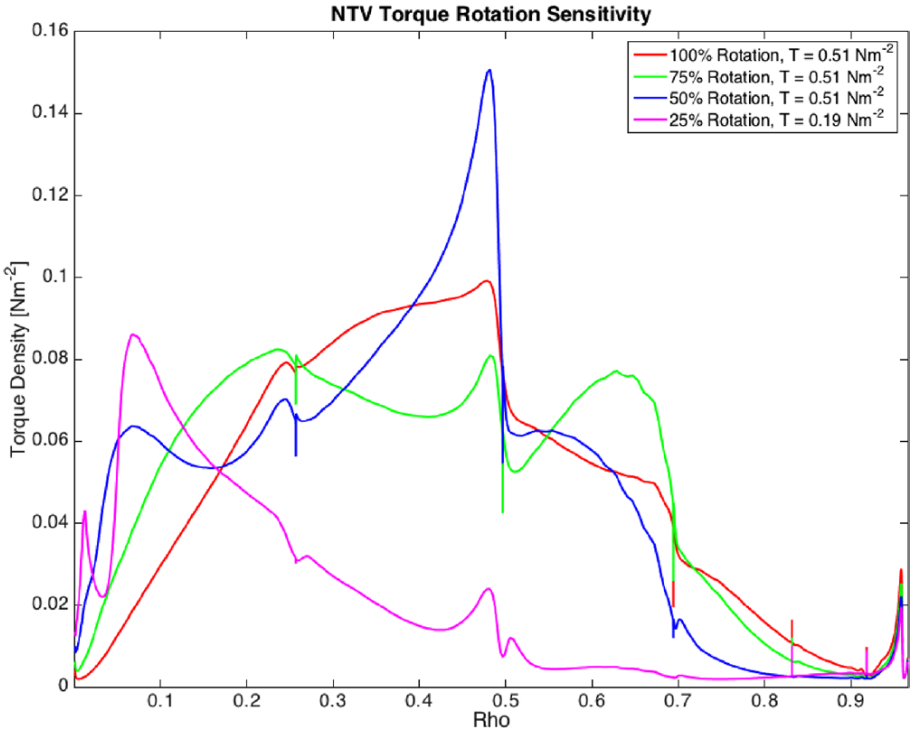

Figure 9. Torque profiles showing sensitivity of profiles to rotation profile. Percentages indicate scaling factor of the original equilibrium (no re-optimization of profiles). Total torque indicated in legend.

systems. In each case the perturbations appear to be pitch non-resonant. This supports the previous statements that the optimizer was attempting to minimize resonant field drive. Both simulations exhibit a strong response near the x-points, which is attributed to plasma response. The large $n = 1$ field amplitude on the inboard side of the plasma are also attributed to plasma response. These results suggest that significant core and edge torques may be generated by coils located in the low field regions, motivating the optimization of the planned NCC and existing RWM coil currents.

A set of optimizations were then preformed where the as designed coils currents were varied in the RWM and NCC coil sets. The IPEC code requires that only one toroidal mode number be considered at a time. In the linear limit toroidal modes are independent. Thus a waveform in each coil row was chosen such that its fundamental harmonic ($n = 1$ or $n = 3$) was preserved. The resulting parameter space was 6 dimensional as the phase and amplitude of each coil row were varied (upper NCC, RWM and lower NCC). The optimizations indicated reasonable coils currents for all but the $n = 1$ edge case (table 1). This case also failed to produce a meaningful torque profile. This is attributed to penetration of the $n = 1$ fields into the plasma, amplification near the $q = 2$ and $q = 3$ surface and difficulties localizing the response near the edge.

The $n = 1$ core and $n = 3$ edge torque drive results from before were recovered (figure 8). This suggests that the full NCC coil set (along with the RWM coils) are adequate for core and edge torque control. A more interesting result came from an attempt to drive core torque with an $n = 3$ field. This resulted in a relatively broad torque profile somewhere between the previous results. While this profile had approximately half the peak torque density of the other profiles, it also has the lowest applied coil currents. In addition, this profile has resonant structures which were greatly reduced as compared to the $n = 3$ and $n = 1$ cases.

The sensitivity of these calculations to rotation profile is shown in figure 9. In the optimized $n = 1$ NCC/RWM coil configuration the rotation profile has been scaled down and PENT used to recalculate the torque. The profiles become more peaked around the $\rho = 0.5$ surface as rotation decreases. However, the total torque remains fixed, even when the rotation has fallen to half it's original value. Once the rotation drops to the one quarter the original value, the torque becomes much more core peaked, although the total torque is now less than half the original value. This suggests that the calculation of torque will be robust to variations in the rotation profile. The question of equilibrium robustness to variations in rotation is beyond the scope of this work.

4. Discussion

In this work, the first optimizations of perturbed tokamak equilibria are presented for NSTX-U, in which NTV torque serves as the target quantity. The optimizations were preformed numerically by the IPECOPT code using a Levenberg–Marquardt method. This code is based upon the STELLOPT optimizer and utilizes IPEC for perturbed linear ideal MHD equilibria. The NTV torque was calculated by the PENT code allowing for target NTV torque density profiles to be specified. A torque

density scan experiment on DIII-D was replicated with the code using modeled error fields. These numerical results were similar to experimental measurements, suggesting that these codes were capable of modeling experiment. Additionally, mapping of the two-dimensional parameter space of this test problem confirmed that the optimization process was correctly finding the minimum of said space. Optimization of the applied Fourier spectrum in NSTX-U suggested a pitch non-resonant perturbing field to drive NTV torque. Here $n = 1$ fields drove core torque and $n = 3$ fields drove edge torque. An optimization of the coil currents for the planned NSTX-U NCC coil along with the existing RWM coils was then preformed. This corroborated the capabilities of these coils to drive similar torque profiles. Additionally, the $n = 1$ was shown to be ineffective in driving edge torque, while the $n = 3$ was capable of driving a very broad torque profile. These are the first simulations of this type and suggest that more sophisticated approaches to coils design be explored in the future.

It is left to future work to explore more detailed possibilities with this and other codes. While the DIII-D example did suggest that the codes could predict experimental results, the example shown is far from conclusive. These results suggest a future set of experiments in NSTX-U taking advantage of the NCC coils. Such experiments could help us better understand the effects of profile response on the predicted torque profiles and our ability to infer torque profiles from measurements of rotation. The IPECOPT code will also be extended to include additional targets such as flux surface overlap parameters. The IPEC code itself is capable of outputting the eigenvectors associated with island formation. It is then possible to significantly reduce the Fourier space of the problem by working with orthogonal modes rather than directly with Fourier harmonics. This would make it possible to directly target the least-resonant mode. Overall, IPECOPT provides an extendable tool for prediction of perturbed equilibrium effects in tokamaks.

Acknowledgments

The authors would like to thank J Menard, D Gates and A Bhattacharjee for their support of this work. Additionally, they would like to thank A Glasser for access to the DCON code.

References

[1] Menard J E *et al* 2012 Overview of the physics and engineering design of nstx upgrade *Nucl. Fusion* **52** 083015
[2] Spong D A *et al* 2001 Physics issues of compact drift optimized stellarators *Nucl. Fusion* **41** 711–6
[3] Hirshman S P and Whitson J C 1983 Steepest-descent moment method for three-dimensional magnetohydrodynamic equilibria *Phys. Fluids* **26** 3553–68
[4] Park J-K, Boozer A H and Glasser A H 2007 Computation of three-dimensional tokamak and spherical torus equilibria *Phys. Plasmas* **14** 052110
[5] Logan N C, Park J-K, Kim K, Wang Z and Berkery J W 2013 Neoclassical toroidal viscosity in perturbed equilibria with general tokamak geometry *Phys. Plasmas* **20** 122507
[6] La Haye R J, Fitzpatrick R, Hender T C, Morris A W, Scoville J T and Todd T N 1992 Critical error fields for locked mode instability in tokamaks *Phys. Fluids* **4** 2098
[7] Hanson J D 1999 Using external coils to correct field errors in tokamaks *IEEE Trans. Plasma Sci.* **27** 1588–95
[8] Hanson J D 1994 Correcting small magnetic field non-axisymmetries *Nucl. Fusion* **34** 441
[9] Sabbagh S A *et al* 2004 The resistive wall mode and feedback control physics design in NSTX *Nucl. Fusion* **44** 560–70
[10] Sontag A C *et al* 2007 Investigation of resistive wall mode stabilization physics in high-beta plasmas using applied non-axisymmetric fields in NSTX *Nucl. Fusion* **47** 1005–11
[11] Strait E J *et al* 2004 Resistive wall mode stabilization with internal feedback coils in DIII-D *Phys. Plasmas* **11** 2505
[12] Evans T E *et al* 2008 RMP ELM suppression in DIII-D plasmas with ITER similar shapes and collisionalities *Nucl. Fusion* **48** 024002
[13] Evans T E *et al* 2006 Edge stability and transport control with resonant magnetic perturbations in collisionless tokamak plasmas *Nat. Phys.* **2** 419–23
[14] Canik J M *et al* 2010 ELM destabilization by externally applied non-axisymmetric magnetic perturbations in NSTX *Nucl. Fusion* **50** 034012
[15] Suttrop W 2000 The physics of large and small edge localized modes *Plasma Phys. Control. Fusion* **42** 1–A14
[16] Loarte A *et al* 2003 Characteristics of type I ELM energy and particle losses in existing devices and their extrapolation to ITER *Plasma Phys. Control. Fusion* **45** 1549–69
[17] Boozer A H 2001 Error field amplification and rotation damping in tokamak plasmas *Phys. Rev. Lett.* **86** 5059–61
[18] Finken K H *et al* 2007 Influence of the dynamic ergodic divertor on transport properties in TEXTOR *Nucl. Fusion* **47** 522–34
[19] Merkel P 1987 Solution of stellarator boundary-value-problems with external currents *Nucl. Fusion* **27** 867–71
[20] Strickler D J, Berry L A and Hirshman S P 2002 Designing coils for compact stellarators *Fusion Sci. Technol.* **41** 107–15
[21] Glasser A H 1997 The direct criterion of newcomb for the stability of an axisymmetric toroidal plasma *Los Alamos Report* LA-UR-95-528
[22] Piron L *et al* 2013 3d magnetic fields and plasma rotation in rfx-mod tokamak plasmas *Nucl. Fusion* **53** 113022
[23] Grimm R C, Dewar R L and Manickam J 1983 Ideal mhd stability calculations in axisymmetric toroidal coordinate systems *J. Comput. Phys.* **49** 94117
[24] Hastie R J, Taylor J B and Haas F A 1967 Adiabatic invariants and the equilibrium of magnetically trapped particles *Ann. Phys.* **41** 302–38
[25] Park J-k, Boozer A H and Menard J E 2009 Nonambipolar transport by trapped particles in tokamaks *Phys. Rev. Lett.* **102** 065002
[26] Pujol J 2007 The solution of nonlinear inverse problems and the levenberg-marquardt method *Geophysics* **72** W1–6
[27] Goldberg D E 1989 *Genetic Algorithms in Search, Optimization and Machine Learning* (Reading, MA: Addison-Wesley)
[28] Poli R, Kennedy J and Blackwell T 2007 Particle swarm optimization *Swarm Intell.* **1** 33–57
[29] Paz-Soldan C, Lanctot M J, Logan N C, Shiraki D, Buttery R J, Hanson J M, La Haye R J, Park J-K, Solomon W M and Strait E J 2014 The importance of matched poloidal spectra to error field correction in diii-d *Phys. Plasmas* **21** 072503
[30] Schaffer M J, Menard J E, Aldan M P, Bialek J M, Evans T E and Moyer R A 2008 Study of in-vessel nonaxisymmetric ELM suppression coil concepts for ITER *Nucl. Fusion* **48** 024004
[31] NSTX-U Team 2014 The nstx upgrade five year plan *Technical Report* Princeton Plasma Physics Laboratory